Materials and Design 120 (2017) 394–403

Contents lists available at ScienceDirect

Materials and Design

journal homepage: www.elsevier.com/locate/matdes

Effect of sintering pressure on microstructure and mechanical properties of hot-pressed Ti6Al4V-ZrO_2 materials

S. Madeira [a,*], A.M.P. Pinto [a], L.C. Rodrigues [c,d], O. Carvalho [a], G. Miranda [a], R.L. Reis [c,d], João Caramês [b], F.S. Silva [a]

[a] Center for Micro-Electro Mechanical Systems (CMEMS), University of Minho, Campus de Azurém, 4800-058 Guimarães, Portugal
[b] Faculty of Dental Medicine, University of Lisbon, 1649-003 Lisboa, Portugal
[c] B's Research Group - Biomaterials, Biodegradables and Biomimetics, University of Minho, Headquarters of the European Institute of Excellence on Tissue Engineering and Regenerative Medicine, AvePark, 4806-909, Taipas, Guimarães, Portugal
[d] ICVS/3B's - PT Government Associate Laboratory, Braga, Guimarães, Portugal

HIGHLIGHTS

- This study proposes a bilayered materials design approach obtained by hot pressing for biomedical applications.
- The effect of sintering pressure on chemical composition and mechanical properties (namely H and E) was studied.
- Interface reaction and mechanical properties are strongly dependent on sintering pressure.
- The highest hardness and modulus were found for materials produced at P = 100 MPa.
- An interesting blackening phenomenon on ZrO_2 layer was described and discussed in light of the variation of O/Zr ratio.

GRAPHICAL ABSTRACT

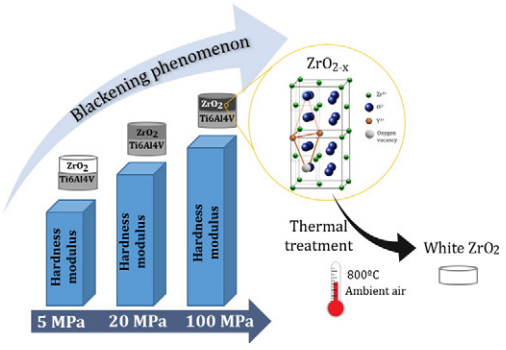

ARTICLE INFO

Article history:
Received 14 December 2016
Received in revised form 30 January 2017
Accepted 13 February 2017
Available online 16 February 2017

Keywords:
Ti6Al4V
ZrO_2
Metal-ceramic
Microstructure
Mechanical properties

ABSTRACT

The development of new design approaches for biomedical applications using conventional and well accepted bio inert materials is an actual challenge. This study proposes a bilayered materials design approach obtained by hot pressing and is concerned with the influence of sintering pressure on the interface reaction between titanium alloy (Ti6Al4V) and zirconia (ZrO_2), on density and mechanical properties of the Ti6Al4V-ZrO_2. For this purpose, different sintering pressures were studied (P = 5, 20 and 100 MPa). Bilayered materials were produced by hot pressing process, at T = 1175 °C. Microstructural characterization showed that Ti6Al4V reacts with ZrO_2 (for P≥20 MPa) and that the interface reaction is strongly dependent on pressure. Additionally, an oxygen-deficient ZrO_{2-x} black zirconia layer was obtained for specimens produced at P = 20 and 100 MPa as result of decreased O/Zr ratio due to Ti diffusion into ZrO_2 side. Young's modulus and hardness properties were evaluated by nano-indentation test. The results showed that these properties are influenced by sintering pressure, increasing with an increase on sintering pressure, with the highest improvement for specimens produced at higher pressure.

* Corresponding author.
E-mail address: saramadeira@dem.uminho.pt (S. Madeira).

http://dx.doi.org/10.1016/j.matdes.2017.02.038
0264-1275/

1. Introduction

Titanium and its alloys are very attractive materials for aerospace and chemical industries due their distinct mechanical properties such as high specific strength (strength to density ratio) [1–4], corrosion resistance [1–5] and strength at relative high temperature [4,6]. Additionally, since *Branemark's* discover these materials are widely used for biomedical applications such as orthopedic and dental applications due to their low weight [5], biocompatibility [2–5] and ability to osseointegrate [4,5] associated to their mechanical properties (toughness and fatigue strength) [7].

Regarding dental rehabilitation, the well documented beneficial results make titanium the gold standard material for the replacement of missing teeth [8]. However, one of drawbacks when using titanium and its alloys is the possibility of metallic ions release, causing hypersensitivity reactions [9].

Zirconia (ZrO_2) is a very attractive ceramic for biomedical applications (such as dental implants and ball heads of femoral implant) due to its high resistance and flexural strength, wear resistance [10], thermal shock resistance [10], biocompatibility [11] and low affinity to bacterial colonization [12,13].

In order to take advantage of both titanium and zirconia, a materials design with zirconia coatings have been used for coating titanium substrate to improve the tribological properties [14] and osteointegration [15]. However, due to shear stresses during implantation or operation, these coatings can be detached from metal surface and thus compromising the function of application. With the development of biomaterials science and industry technology, zirconia was proposed as a new material for hip head replacement and later for dental implants (due to its toothlike color) instead of titanium. However, ceramics are known to be sensitive to shear and tensile loading which imply a high risk of fracture [8].

In this context, the development of Ti6Al4V-ZrO_2 bilayered materials produced by hot pressing seems to present an advantageous and original combination of materials and process for biomedical applications to surpass the disadvantages of the current solutions.

In the past decades, several studies have been conducted investigating the interfacial reaction between pure Ti and ZrO_2 [16–23]. Many of these studies performed at elevated temperatures indicated that distinct reaction layers can be formed at the interface. Furthermore, these studies indicated that oxygen-deficient and blackened ZrO_2 was formed as result of oxygen dissolution into Ti. Lin and Lin [24] studied the diffusional reaction between Ti and ZrO_2 at different temperatures (1100, 1300, 1400 and 1550 °C). They reported that interface is strongly dependent on temperature and that at T = 1100 °C the limited reaction resulted in $t\text{-}ZrO_{2-x}$. Lin and Lin [23] studied ZrO_2-Ti composites produced by hot pressing, for thermal barrier graded materials, reporting that at higher sintering temperatures (1500 °C), Ti reacts with and is mutually soluble in ZrO_2, resulting in the formation of oxides (such as α-Ti(O, Zr), Ti_2ZrO and/or TiO) which is dependent on Ti/ZrO_2 ratio. Teng and co-workers [25] describe that a phase transformation of zirconia (from tetragonal to monoclic) was found with increase of Ti volume fraction in the composites. Similar results were obtained by Lindong Teng and co-workers [26]. Furthermore, Correia et al. [18] studied the microstructure of diffusional zirconia-titanium and zirconia-Ti6Al4V alloy joints, reporting that at higher temperatures (T > 1300 °C), a weak oxide layer is developed from the direct ZrO_2-Ti joints.

Another study conducted by Teng et al. [25] described that no reaction product was formed between Ti and ZrO_2, and that interface bonding state is physical, for Ti-ZrO_2 interfaces fabricated by hot pressing.

Table 2
Chemical composition of 3Y-TZP powder (according to manufacturer).

Element	Y_2O_3	$ZrO_2 + HfO_2 + Y_2O_3 + Al_2O_3$ [a]	Al_2O_3	SiO_2	Fe_2O_3	Na_2O
Wt%	5.15 ± 0.2	>99.9	0.25 ± 0.1	≦0.02	≦0.01	≦0.04

[a] Calculated value − 100 − ($SiO_2 + Fe_2O_3 + Na_2O$).

Even though extensive studies were carried out on the interface reactions, the pressure effect on the microstructure evolution (including blackening phenomenon on ZrO_2) and mechanical properties (hardness and Young's modulus), at T = 1175 °C, for solid-state Ti6Al4V-ZrO_2 materials produced by hot pressing, were not studied to date.

Regarding this processing technology, a hot-pressing method was used because it allows the manufacturing of near-net-shape products with near full densification, therefore eliminating finishing operations [6].

2. Materials and methods

2.1. Materials

In this study, Ti6Al4V alloy spherical powder (TLS Technik GmbH & Co. Spezialpulver KG) with average particle diameter of 45 μm and commercial Yttria-stabilized zirconia (3Y-TZP) powder with uniform dispersion of 3 mol% Yttria (Tosoh Corporation) constituted by spherical granules (having an average diameter of 60 μm) of much smaller crystals that are about 40 nm in diameter. The chemical composition of titanium alloy and zirconia are presented in Tables 1 and 2, respectively. Scanning electron microscopy (SEM) images of Ti6Al4V and 3Y-TZP (in agglomerate form) powders are presented in Fig. 1a) and b), respectively.

Fig. 2 shows Ti6Al4V and 3Y-TZP powders size distribution (according to manufacturer), showing that 90% of the Ti6Al4V and 3Y-TZP powders have a diameter below 47.64 μm (Fig. 2a) and 90 μm (Fig. 2b), respectively.

2.2. Fabrication of Ti6Al4V-ZrO_2 bilayered materials

Ti6Al4V-ZrO_2 bilayered (metal-ceramic) materials were produced by powder metallurgy (PM) process, namely hot pressing (HP), under vacuum (10^{-2} mbar) at different conditions, being shown along with respective sample codes in Table 3. The samples processed at varying pressures have been marked as TZ-P, followed by the respective pressure value.

The sintering temperature (T = 1175 °C) was chosen based on previous works concerning Ti6Al4V produced by hot pressing and also taking into account the near full densification of ZrO_2 and the reaction between Ti and ZrO_2. Regarding the Ti6Al4V sintering temperature, there are some studies that reported near full densification at T = 1100 °C using hot pressing [4,6,26,27]. In case of ZrO_2, higher sintering temperatures (T = 1350–1550 °C, according to supplier – Tosoh Corporation) are required for conventional sintering processes. However, when using pressure (as in hot pressing), it is possible to compensate temperature with pressure, thus allowing to sinter at lower temperatures. Bernard-Granger et al. [28] reported full densification (99.5%) of ZrO_2 at T = 1150 °C, during 15 min, using 100 MPa. Concerning the reaction between Ti and ZrO_2, Teng et al. [10,25] studied

Table 1
Chemical composition of Ti6Al4V alloy powder (according to manufacturer).

Element	Ti	Al	V	C	Fe	O	N	H	Y	Zn	Mg
Wt%	Bal.	6.2	4.1	0.02	0.19	0.13	0.01	0.001	<0.001	<0.001	<0.001

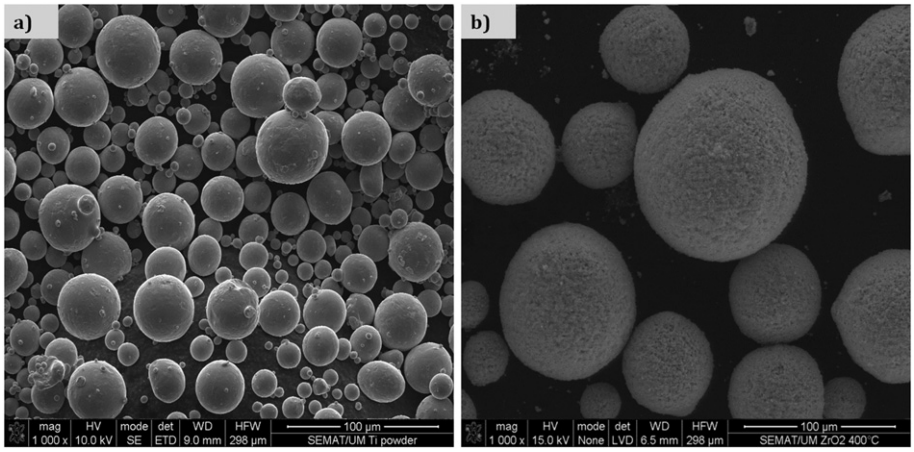

Fig. 1. SEM images of a) Ti6Al4V alloy powder and b) 3Y-TZP powder.

thermodynamics and microstructure of Ti-ZrO_2 metal-ceramic functionally graded materials produced by hot pressing under the temperature range 1200–1400 °C, and they reported that no obvious reaction between Ti and ZrO_2 was found.

The titanium alloy powder was placed inside graphite mould (painted with ZrO_2 in order to prevent carbon diffusion to specimen). Then, the zirconia powder was applied onto titanium powder and sintered by means of pressure-assisted sintering process (HP), using a high frequency induction furnace, as schematically represented in Fig. 3. The mould was placed inside the chamber, where both pressure and temperature were increased till reaching the targeted values. These conditions were maintained during dwelling stage. Then, the samples were cooled till room temperature at cooling rate of 15 °C/min, without pressure. All obtained samples had average diameter of 8 mm.

After sintering process, the Ti6Al4V-ZrO_2 bilayered specimens were cut and there cross sections polished.

2.3. Microstructural and chemical characterization

Selected samples were sectioned and polished for microstructural characterization by means of Scanning Electron Microscopy (SEM) equipped with an Energy Dispersive Spectrometer (EDS). X-ray diffraction (XRD) analysis was performed for phase identification (crystalline structure) using a Bruker AXS D8 Discover diffractometer with a Cu-Kα radiation (λ = 1.54,060 Å). The 2θ was measured from 20° to 85° with a stepsize of 0.04° and a steptime of 1 s.

2.4. XPS analysis

X-ray photoelectron spectroscopy (XPS) was performed to study the changes of the bonding environment of Zr and O at the zirconia layer. The chemical composition of 6 samples was examined by XPS surface measurements. The C1s, O1s, Zr3d and survey spectra were recorded using a Kratos Axis-Supra instrument. Monochromatic X-ray source Al Kα (1486.6 eV) was used for all samples and experiments. The X-ray Monochromatic spot is 500 mm Rowland circle diameter and the residual vacuum in the analysis chamber was maintained at around 9×10^{-9} Torr. The samples were fixed to the sample holder with double sided carbon tape.

The binding energies (BEs) positions were referenced to the C1s on unsputtered surfaces. Charge referencing was done by setting the binding energy of C1s photo peak at 285.0 eV C1s hydrocarbon peak. Furthermore, an electron flood gun was employed to minimize surface charging (charge compensation). The atomic concentrations were determined from the XPS peak areas using the Shirley background subtraction technique and the Scofield sensitivity factors.

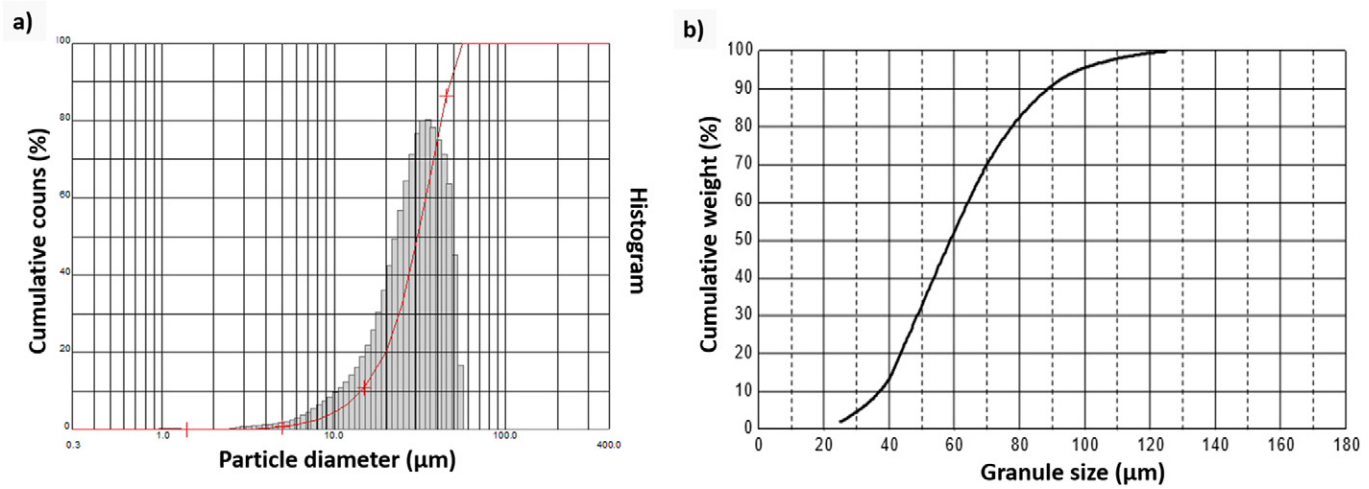

Fig. 2. a) Ti6Al4V powder size distribution (according to TLS Technik) and b) 3Y-TZP powder, granule size distribution (according to Tosoh Corporation).

Table 3
Summary of HP parameters studied.

Sample code	Sintering parameters			
	Temperature (°C)	Heating rate (°C)/min	Pressure (MPa)	Dwell time (min)
TZ-P5	1175	117.5	5	15
TZ-P20	1175	117.5	20	15
TZ-P100	1175	117.5	100	15

2.5. Density evaluation

The density of the obtained samples was measured through image analysis by means of *ImageJ* software. In this context, a threshold filter was previously applied by means of Adobe Photoshop software in order to obtain black and white images. The black areas represent the pores while white area consists to the densified area. For each sample, six different zones were analyzed and the densified area was calculated. The average results for each condition are designated as relative density (%).

2.6. Nanoindentation tests

The hardness (H) and Young's modulus (E) of the Ti6Al4V-ZrO_2 samples were measured in cross section by means of a nanoindenter equipment (NanoTest - Micro Materials), using a Berkovich diamond indenter type. A line of indentations (with a 20 μm between each indentation) was made to a maximum load of 120 mN. Hardness and elastic modulus profiles were obtained across metal-ceramic zone from the load-displacement curves. The Young's modulus (E) of materials (Ti6Al4V and zirconia) was calculated by using Eq. (1) [29].

$$\frac{1}{E_r} = \frac{1-\nu_i^2}{E_i} + \frac{1-\nu_m^2}{E} \quad (1)$$

where E_i and ν_i are the elastic modulus and Poisson ratio of the diamond indenter, respectively. $E_i = 1141$ GPa and $\nu_i = 0.07$

3. Results and discussion

3.1. Microstructural and chemical characterization

Fig. 4A), B) and C) show a schematic representation of the produced Ti6Al4V-ZrO_2 bilayered materials revealing a blackening effect on zirconia layer with increasing pressure. Furthermore, a decrease of sample height with increasing sintering pressure can be observed, indicating a higher densification level for higher pressures.

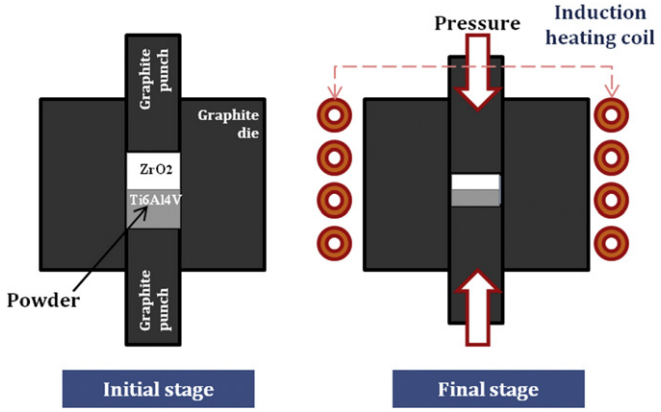

Fig. 3. Hot pressing schematic representation.

Similar to conventional sintering processes, HP sintering is comprised by four stages: activation and rearrangement of particles, connection of particles, growth of sintering neck and bulk deformation [30]. The only difference is that HP is a sintering method that involves the application of mechanical pressures with heating to accelerate densification.

According to Munir and co-workers [31], the effect of pressure on sintering of Ti can be divided into intrinsic and extrinsic effects. The intrinsic effects involve diffusion-related material transport, viscosity flow, plasticity transformation, and creep process, while the extrinsic effect of pressure corresponds to a particle rearrangement and collapse of particle agglomerates.

Regarding the effect of pressure on ZrO_2 densification, Bernard-Granger and co-workers [28] reported two mechanisms (based on densification law derived from creep rate equations and TEM analysis) that can be invoked during densification of the powder using HP, whatever the temperature: for high effective pressures (such as P = 100 MPa), densification proceeds by grain boundary sliding accommodated by grain boundary diffusion of the Zr4+ and/or Y3+ cations; and for lower effective pressures (such as P = 5 MPa), densification proceeds by grain boundary sliding accommodated by an in-series (interface-reaction/lattice diffusion of the Zr4+ and/or Y3+ cations) mechanism controlled by the interface-reaction step.

Fig. 4(D–I) show the micrographs of the polished Ti6Al4V-ZrO_2 bilayered materials for different pressures. The micrographs revealed an improvement in the density as consequence of pressure increase.

Regarding specimens produced at P = 5 MPa, porosity is visible, especially in the zirconia layer. When comparing the micrographs of TZ-P20 with TZ-P5, a decrease in porosity is achieved. For TZ-P100 specimens, a great improvement in densification occurred assessing the effectiveness of the hot pressing process for the production of these materials.

SEM-EDS line scans were carried out by EDS, and the scan regions are shown in Fig. 4(J–L), revealing that inter-diffusion of some elements occurred between the two materials. Elements constituting the titanium alloy (e.g. Ti, Al and V) were found in the vicinity of the interface (especially Ti). Regarding vanadium (V), no significant diffusion was found. On the other hand, Oxygen (O) of ZrO_2 was the one that most diffused. A remark should be made relatively to aluminum (Al) concentration at the interface zone of TZ-P100 (Fig. 4L). It is possible to see that there was a greater diffusion of Al (reaching ≈20 at.%) using P = 100 MPa, when compared to diffusion at lower pressures (reaching ≈10 at.%).

Fig. 4(J–L) also shows that interface reaction between Ti6Al4V alloy and the ZrO_2 took place for samples sintered at P = 20 MPa and P = 100 MPa. Regarding 5 MPa, no significant interface reaction zone was found. Furthermore, from Fig. 4(G–I) it is possible to see that the reaction between titanium alloy and zirconia strongly depends on pressure. Furthermore, the extent of the interface reaction changed and increased with pressure increase (≈2 μm for TZ-P20 and ≈26 μm for TZ-P100). In TZ-P20, a monophasic and discontinuous interface layer is formed, while in TZ-P100 different reaction zones (different phases) can be observed.

Table 4 shows the results obtained by EDS analysis, performed in the interface zones of TZ-P20 and TZ-P100. When comparing reaction zone of TZ-P20 (marked as A in Fig. 4H) with reaction zones of TZ-P100 (marked as B, C and D in Fig. 4I), it is possible to see that a great amount of oxygen is presented at the interface reaction zones of TZ-P100 specimens (especially B and D zones), when compared with TZ-P20 specimens (A zone), indicating higher reduction of ZrO_2. Furthermore, a greater Al content (see Table 4) was found for darker zones (D zone).

As it is known, the interface reaction has an important role in the structure and mechanical properties. An insufficient interface diffusion can result to a poor interfacial bonding. With pressure increase the diffusion of elements increase as well as the extent of reaction. Depending on products reaction, the interface formed can improve mechanical properties of materials or be detrimental.

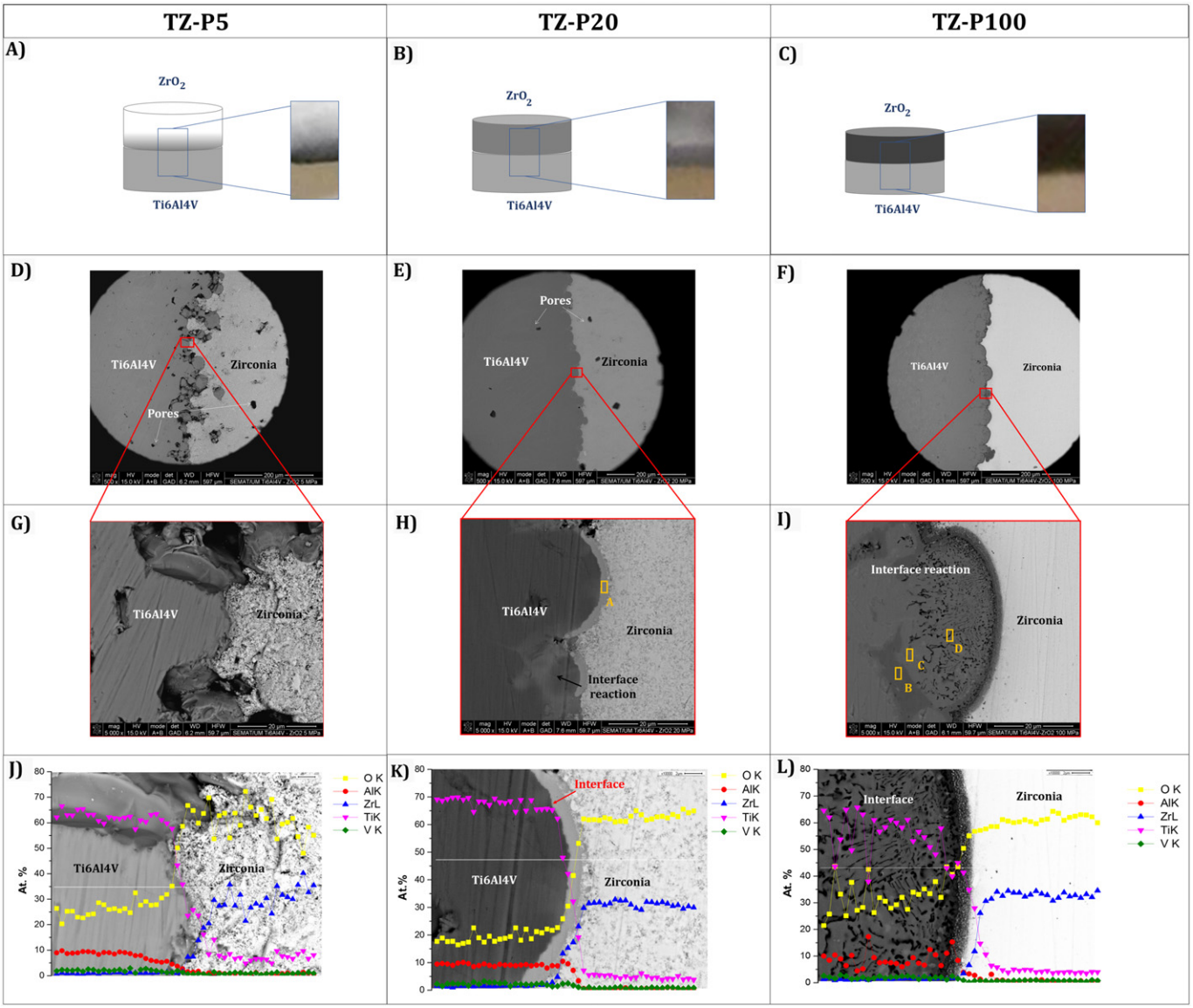

Fig. 4. Schematic representation (A, B and C) and SEM micrographs (D–I) of Ti6Al4V-ZrO_2 bilayered materials sintered at different pressures (5, 20 and 100 MPa) with SEM-EDS line scan analysis (J, K and L).

XRD analysis (see Fig. 5) were performed at the interface zone of TZ-P100 specimens (greater extension of reaction) to evaluate the possible formed phases and thus predict the behavior of interface. The results showed hexagonal Ti and tetragonal ZrO_2 peaks and no peaks of titanium oxides were found. Considering that it is possible to control the interface reaction by controlling the pressure and by this way tailor the properties of materials for a specific application, further characterizations of interface (such as shear bond strength) are being performed by the authors.

Table 4
Chemical composition (in wt.%) interface of TZ-P20 (marked in Fig. 4H)) and TZ-P100 (marked in Fig. 4I)) obtained in polished cross section surface, by EDS.

TZ-P20	A	TZ-P100	B	C	D
Ti	51.78	Ti	83.33	79.75	46.99
Al	6.36	Al	1.02	3.94	16.36
V	2.39	V	0.00	3.13	1.86
Zr	30.03	Zr	3.53	3.42	3.30
O	9.45	O	12.12	9.76	31.49

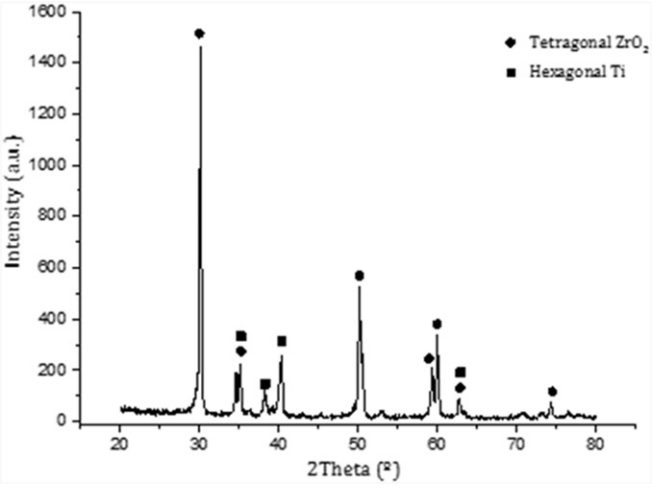

Fig. 5. XRD spectra of TZ-P100 interface zone.

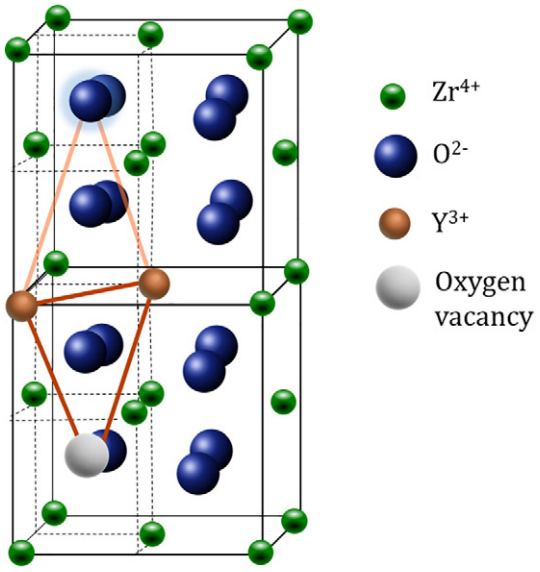

Fig. 6. Schematic representation of oxygen vacancy of a trimer in yttria stabilized tetragonal zirconia.

3.2. Blackening phenomenon of ZrO_2

A change in color of ZrO_2 (from white to gray black) was observed when sintered with Ti6Al4V. This observation is in line with other study regarding zirconia to Ti6Al4V braze joint for implantable biomedical device [32]. The blackening effect depends on the applied pressure (considering the same temperature and dwelling time). An interesting observation is that this color change or blackening effect starts in the interface zone (direct contact with Ti6Al4V), as can be seen from Fig. 4A.

Some studies [16,17,19] regarding interfacial reactions between molten Ti and ZrO_2 have shown that ZrO_2 can be partially reduced to ZrO_{2-x} by Ti through the formation of oxygen vacancies on the zirconia structure (schematically represented in Fig. 6). Since the diffusivity of oxygen (O) in Ti is much faster than that of zirconium (Zr) and Ti has a great affinity with O [16], an oxygen deficient Zirconia accompanied by a dark gray color can be formed [16,19]. Although a small interface extent was formed (maximum 26 μm), a color change was observed in the entire layer.

Contrarily to other studies [16] where a transformation phase of ZrO_2 with oxygen content reduction (Black zirconia) was reported, in this work it is possible to conclude from XRD pattern (Fig. 7) for TZ-P5, TZ-P20 and TZ-P100 (performed at the ZrO_2 layer) that the structure of ZrO_2 after sintering (Black zirconia) is not affected by blackening phenomenon, once that no transformation phase occurs.

According to the application, the color of the ZrO_2 can be decisive for the use or not of this material. For example, white ZrO_2 is required for dental applications (where aesthetic properties are very important) while for hip prostheses blackened ZrO_2 can be accepted. In order to support explanation of blackening phenomenon conducted by XPS analysis and thus find ways to prevent it, a thermal treatment at 800 °C during 1 h with a heating rate of 5 °C/min was performed in TZ-P100 samples (where color change was observed in the entire

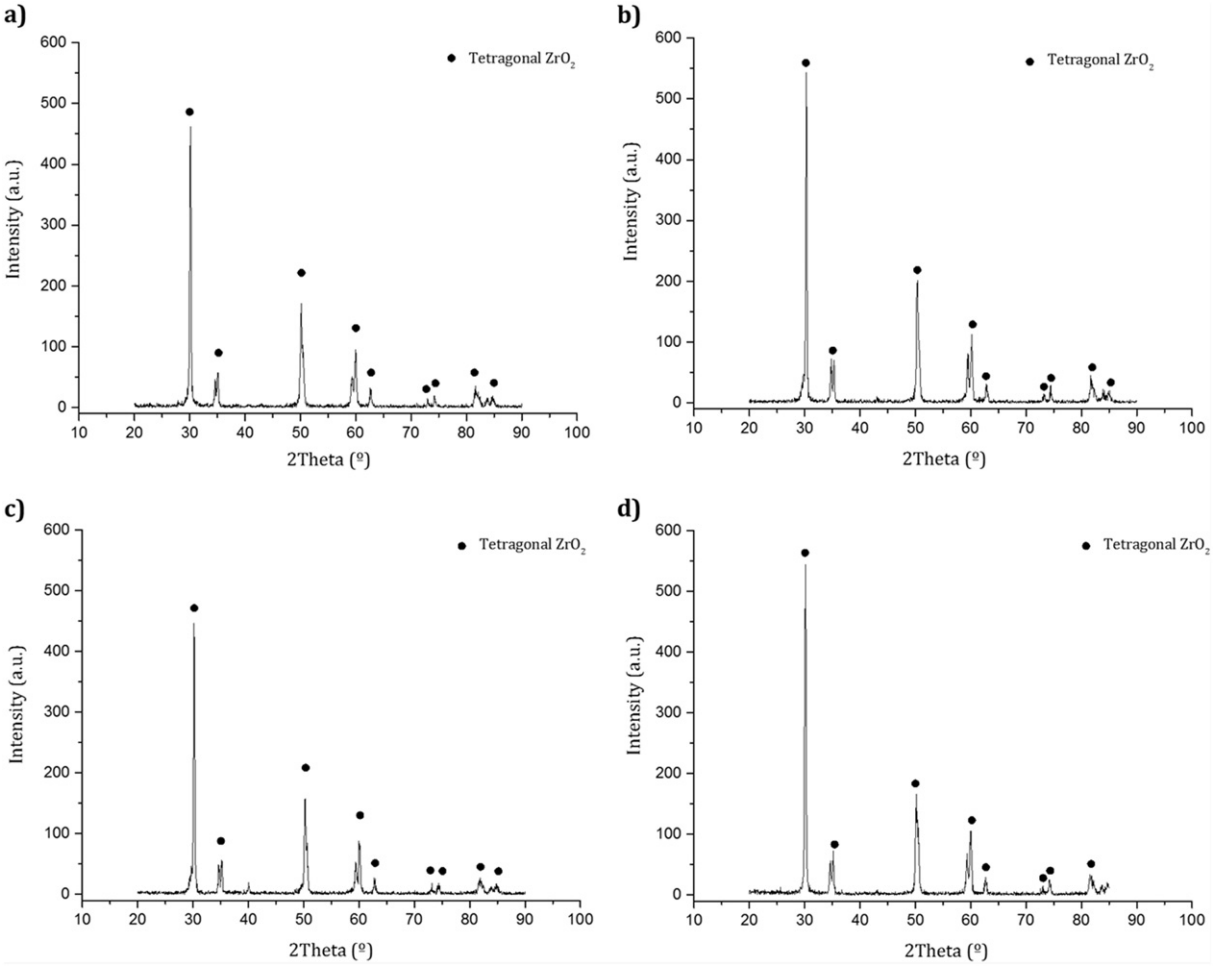

Fig. 7. XRD spectra of (a) TZ-P5, (b) TZ-P20, (c) TZ-P100 and (d) White ZrO_2.

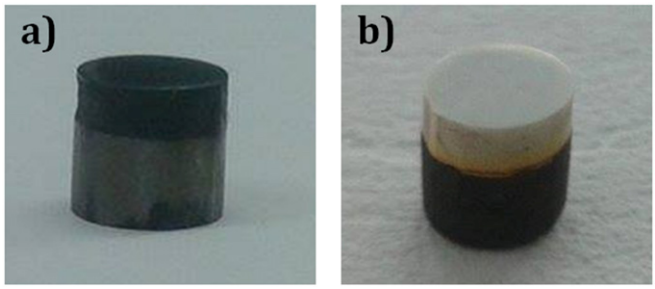

Fig. 8. Photograph of (a) Black ZrO_{2-x} and (b) White ZrO_2 sample after thermal treatment.

layer). Photograph images of samples before (designated as Black ZrO_{2-x}) and after thermal treatment (design as White ZrO_2) are shown in Fig. 8. As can be seen from Fig. 8, when the Black ZrO_2 samples are heated in air (i.e. temperature and oxygen), zirconia becomes white. At same time, as expected, during this treatment Ti6Al4V is exposed to ambient air and oxidizes (although not desired).

Additionally, X-ray photoelectron spectroscopy (XPS) was performed in order to study the alteration of the bonding environment of Zr and O at the surface of ZrO_2 samples with black and white colorations. The high resolution XPS spectrum of Zr 3d region of Black ZrO_2 (Fig. 9A_2) present two bands 181.2 and 183.5 eV which are in accordance with bands at 181.3 and 183.6 eV of White ZrO_2 (Fig. 9B_2) corresponding to 3d electrons of suboxides $Zr^{(4-x)+}$ [33]. Similarly, to other reports, none of the samples present any indication for the presence of metallic Zr (~178 eV) [34,35].

Moreover, the regions spectra of White ZrO_2 sample show, in addition to suboxides, also ZrO_2 contribution, probed by the two more bands appearance which are related to Zr^{4+} electrons [33]. This is in accordance with the high-resolution O1s XPS region spectrum. On deconvolution of this spectrum (Fig. 9B2) it is resolved into three distinguishable bands centered at 530.6, 532.7 and 535.1 eV, corresponding to the oxygen involved on sub-oxides and oxides formation.

Table 5
XPS atomic quantification of O, Y and Zr in the samples.

Sample	%O	%Zr	%Y	O/Zr
White ZrO_2	65.55 ± 0.18	27.71 ± 0.18	6.74 ± 0.18	2.37
Black ZrO_2	49.01 ± 0.17	47.67 ± 0.17	5.47 ± 0.17	1.03

Taking into account the quantification data included in Table 5, it is possible to confirm that the thermal treatment of the samples promoted differences in the chemical composition at the sample surface revealed as an increase of the oxygen content into the sample, which are in accordance with the XPS spectroscopic data. From these results, it is possible to conclude that during sintering process ZrO_2 becomes black as result of the variation on oxygen content in ZrO_2 due to the diffusion of Ti. This information is in line with heat treatment explanation.

Additionally, based on results obtained by Jiang and co-workers [32] for an implantable medical device where blackening phenomenon was reported, it is expected that the biochemical properties of ZrO_2 is not be affect by blackening phenomenon.

3.3. Density

The density was evaluated for three different Ti6Al4V-ZrO_2 sintering pressures (TZ-P5, TZ-P20 and TZ-P100). Fig. 10 shows the relative density as a function of sintering pressure.

Analyzing Fig. 10, relative density values increase with increasing pressure for both materials. From P = 5 MPa to P = 20 MPa, a slight increase on density is observable for Ti6Al4V, while an expressive gain is obtained for ZrO_2. For higher pressures, a slight increase on density was obtained for both materials (metal and ceramic). Furthermore, for a similar pressure Ti6Al4V presents higher densification values when compared with ZrO_2, indicating that the pressure has a great influence in density for ceramic material.

Additionally, it can be seen that relative density values reached at P = 20 and P = 100 MPa are very similar for both materials

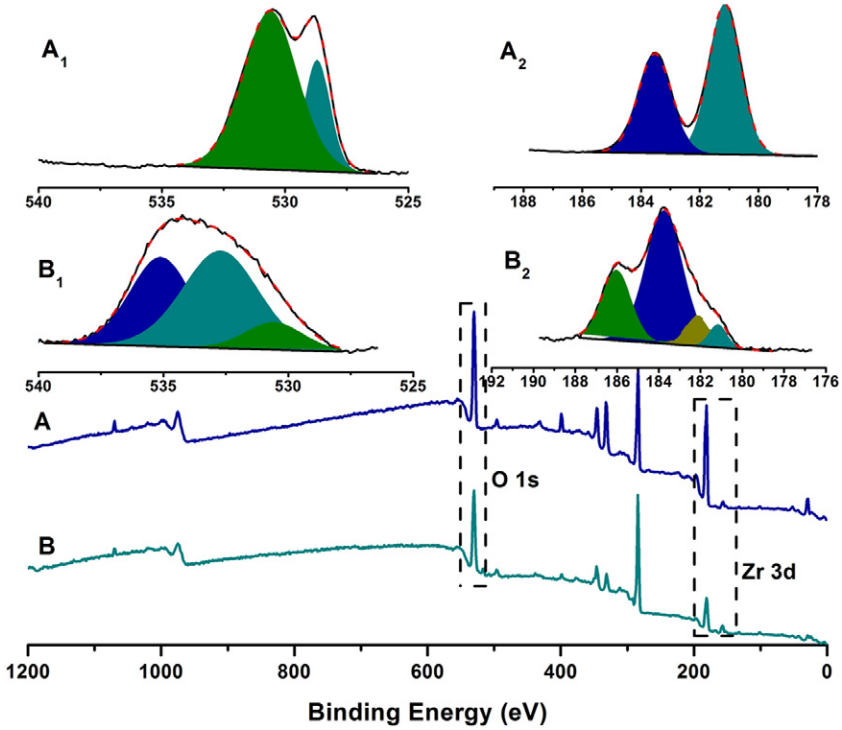

Fig. 9. XPS wide spectrum of ZrO_2 A - Black Sample, B - White Sample; Inset region spectrums of O region (A_1 - Black Sample, B_1 - White Sample) and Zr region (A_2 - Black Sample, B_2 - White Sample).

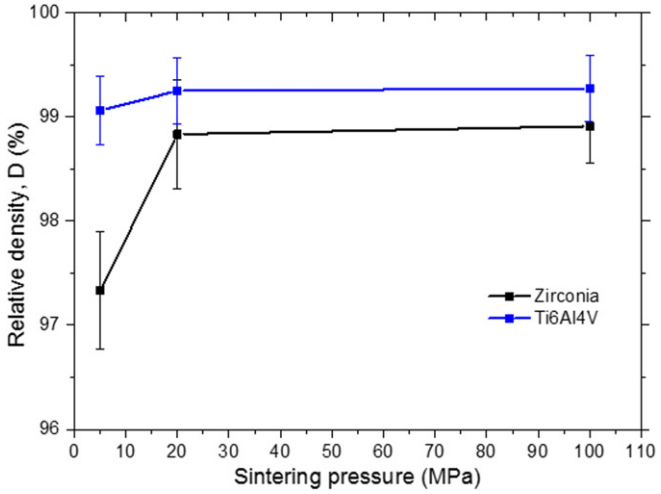

Fig. 10. Densification curves as function of the sintering pressure for zirconia and Ti6Al4V layers.

since they vary between 98.5% and 99%. Therefore, it seems that hot pressing process could be used to produce fully dense Ti6Al4V-ZrO_2 materials.

3.4. Nanoindentation

Nanoindentation tests were performed to assess the influence of sintering pressure on mechanical properties, namely hardness and Young's modulus of Ti6Al4V-ZrO_2 bilayered materials. Fig. 11(a) shows load-displacement curves and correspondent measured values (Fig.11(b)) for TZ-P100. The same approach was done for P = 5 MPa and P = 20 MPa. It is known that the size of penetration depth is related with hardness of each material. Regarding the load-displacement curves for Ti6Al4V-ZrO_2 bilayered, all of them presented the highest penetration depths and lower slopes for titanium when compared to zirconia, as expected due to ductility of titanium alloy.

Table 6 displays average H and E test results as function of the tested pressures (5, 20 and 100 MPa). Table 6 shows the increase of the H and E measured values (for both materials) with increasing sintering pressure, meaning that these mechanical properties can be improved by using higher pressures.

Concerning the comparison between the ZrO_2 and Ti6Al4V materials, it can be noticed that the effect of higher pressures on H and E seems to be higher for zirconia compared to titanium alloy, which is most probably correlated with the adequate sintering temperature for each material. The melting temperature of Ti6Al4V and ZrO_2 are 1604–1660 °C and 2715 °C, respectively. At 1175 °C (approximately of 0.8 of melting point) Ti may undergo plastic deformation even at low

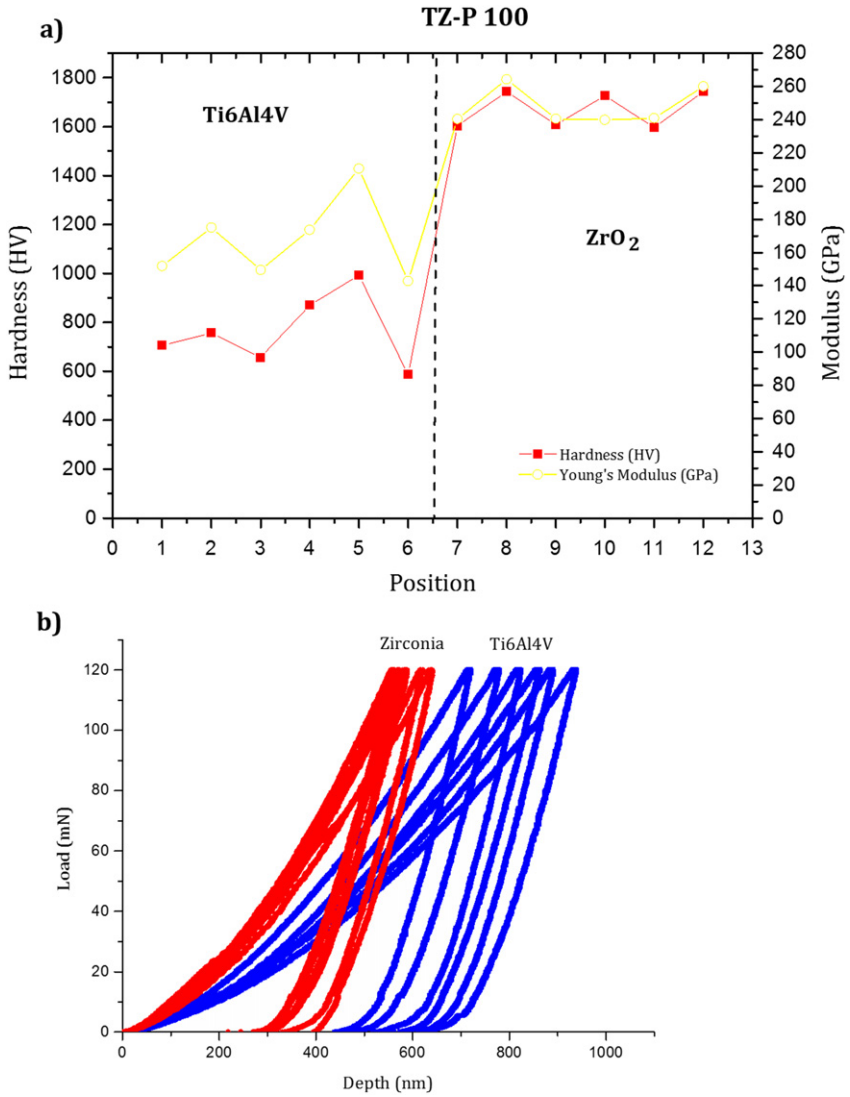

Fig. 11. (a) Measured hardness and modulus and (b) corresponding load-displacement curves for TZ-P100 specimen.

Table 6
Hardness and Young's modulus of Ti6Al4V-ZrO_2 composites produced at different pressures.

	Hardness (HV)		Young's modulus (GPa)	
	Ti6Al4V	ZrO_2	Ti6Al4V	ZrO_2
TZ-P5	558.95	491.39	139.93	121.08
TZ-P20	728.89	533.88	147.10	124.66
TZ-P100	747.35	1683.33	162.48	249.11

pressures, while zirconia requires higher pressures to deform and consolidate, once this temperature is below of adequate sintering temperature.

As shown in Table 6, the obtained hardness and Young's modulus values of Ti6Al4V (for all tested pressures) are higher compared to the literature values assessed by other means than nanoindentation [6,9] probably due to the dissolution of oxygen and/or the titanium oxidation that was originated from ZrO_2 layer [16]. This observation is in line with the results reported by Correia et al. [18].

Ti6Al4V is a $(\alpha + \beta)$ two-phase alloy. However, this structure can be changed according to process used to produce samples (which includes temperature, pressure, time and cooling rate). It is known from literature [36] that the microstructure and mechanical properties are greatly influenced by the cooling rate. Ahmed and co-workers [37] studied phase transformations during cooling in $\alpha + \beta$ titanium alloys and they reported that the results of phase transformation of $\alpha + \beta$ titanium from elevated temperature vary with cooling rate (from 525 to 1.5 °C/s). They also reported that cooling rates between 1.5 °C/s and 20 °C/s induce the transformation of β phase to α phase. According to Esmaily et al. [36], when faster cooling rates take place, a significant improvement of the tensile strength and hardness of Ti6Al4V alloy can be attributed to the presence of martensitic phase. The produced samples experienced a lower cooling rate of (15 °C/min = 0.25 °C/s), indicating that the hardness values were not significant affected by the cooling rate. This observation is in accordance with results reported by [36].

Additionally, the elastic modulus measurement by nanoindentation depends on the selection of the location of the indentation in the microstructure and the size of the microstructural constituents at nanoscale. An inhomogeneity in the microstructure can lead to a considerable variation [38]. This aspect can also explain the enhancement in this material modulus.

Regarding ZrO_2, as seen in Table 6, the results demonstrate that the hardness and Young's modulus of ZrO_2 sintered at P = 100 MPa (considering near full densification) are similar to the literature reported values [39,40], while for lower pressures the obtained values are lower.

4. Conclusions

From the present study, the following conclusions can be drawn:

- This study confirms that hot pressing process could be used to produce fully dense Ti6Al4V-ZrO_2 materials.
- Chemical composition and mechanical properties (hardness and Young's modulus) showed to be strongly dependent on sintering pressure. It was demonstrated that by increasing the sintering pressure, a reaction zone between Ti6Al4V alloy and ZrO_2 as well as a color change on ZrO_2 were found. Furthermore, an improvement in H and E is attained by increase pressure.
- XPS results proved that during sintering process, ZrO_2 was reduced to oxygen-deficient zirconia (ZrO_{2-x}). Furthermore, an increase on the content of oxygen in ZrO_2 in order to obtain white ZrO_2 can be attained by a thermal treatment.

Acknowledgements

This work is supported by FTC through the grant SFRH/BD/112280/2015 and the reference project UID/EEA/04436/2013, by FEDER funds through the COMPETE 2020 – Programa Operacional Competitividade e Internacionalização (POCI) with the reference project POCI-01-0145-FEDER-006941, and NORTE-01-0145-FEDER-000018-HAMaBICo.

References

[1] K.-L. Lin, C.-C. Lin, Ti_2ZrO phases formed in the titanium and zirconia interface after reaction at 1550 °C, J. Am. Ceram. Soc. 88 (2005) 1268–1272.
[2] J.I. Polmear, Titanium alloys light alloys [M], fourth ed. Butterworth-Heinemann, Oxford, 2005 299–365.
[3] H.J. Rack, J.I. Qazi, Titanium alloys for biomedical applications, Mater. Sci. Eng. C 26 (2006) 1269–1277.
[4] L. Bolzoni, E.M. Ruiz-Navas, E. Neubauer, E. Gordo, Inductive hot-pressing of titanium and titanium alloy powders, Mater. Chem. Phys. 131 (3) (2012) 672–679.
[5] A. Dudek, M. Klimas, Composites based on titanium alloy Ti–6Al–4V with an addition of inert ceramics and bioactive ceramics for medical applications fabricated by spark plasma sintering (SPS method), Mater. Werkst. 46 (2015) 237–247.
[6] L. Bolzoni, I. Montealegre Meléndez, E.M. Ruiz-Navas, E. Gordo, Microstructural evolution and mechanical properties of the Ti–6Al–4V alloy produced by vacuum hot-pressing, Mater. Sci. Eng. A 546 (2012) 189–197.
[7] T. Traini, C. Mangano, R.L. Sammons, F. Mangano, A. Macchi, A. Piattelli, Direct laser metal sintering as a new approach to fabrication of an isoelastic functionally graded material for manufacture of porous titanium dental implants, Dent. Mater. 24 (2008) 1525–1533.
[8] Z. Özkurt, E. Kazazoglu, Zirconia dental implants: a literature review, J. Oral Implantol. 37 (2011) 367–376.
[9] R.B. Osman, M.V. Swain, A critical review of dental implant materials with an emphasis on titanium versus zirconia, Materials 8 (3) (2015) 932–958.
[10] L. Teng, W. Li, F. Wang, Effect of Ti content on the martensitic transformation in zirconia for Ti–ZrO_2 composites, J. Alloys Compd. 319 (2001) 228–232.
[11] M. Inokoshi, F. Zhang, J.D. Munck, S. Minakuchi, I. Naert, J. Vleugels, B. Van Meerbeek, K. Vanmeensel, Influence of sintering conditions on low-temperature degradation of dental zirconia, Dent. Mater. 30 (6) (2014) 669–678.
[12] P.F. Manicone, P.R. Iommetti, L. Raffaelli, An overview of zirconia ceramics: basic properties and clinical applications, J. Dent. 35 (11) (2007) 819–826.
[13] L. Rimondini, L. Cerroni, A. Carrassi, P. Torriceni, Bacterial colonization of zirconia ceramic surfaces: an in vitro and in vivo study, Int. J. Oral Maxillofac. Implants 17 (6) (2002).
[14] S. Sathish, M. Geethaa, S.T. Aruna, N. Balaji, K.S. Rajam, R. Asokamani, Sliding wear behavior of plasma sprayed nanoceramic coatings for biomedical applications, Wear 271 (5) (2011) 934–941.
[15] P. Dahl, I. Kaus, Z. Zhao, M. Johnsson, M. Nygren, K. Wiik, T. Grande, M.-A. Einarsrud, Densification and properties of zirconia prepared by three different sintering techniques, Ceram. Int. 33 (8) (2007) 1603–1610.
[16] K.F. Lin, C.C. Lin, Interfacial reactions between Ti-6Al-4V alloy and zirconia mold during casting, J. Mater. Sci. 34 (1999) 5899–5906.
[17] K.F. Lin, C.C. Lin, Interfacial reactions between zirconia and titanium, Scr. Mater. 39 (1998) 1333–1338.
[18] R.N. Correia, J.V. Emiliano, P. Moretto, Microstructure of diffusional zirconia–titanium and zirconia–(Ti–6 wt% Al–4 wt% V) alloy joints, J. Mater. Sci. 33 (1998) 215–221.
[19] J. Zhu, A. Kamiya, T. Yamada, W. Shi, K. Naganuma, K. Mukai, Surface tension, wettability and reactivity of molten titanium in Ti/yttria-stabilized zirconia system, Mater. Sci. Eng. A 327 (2002) 117–127.
[20] Y.W. Chang, C.C. Lin, Compositional dependence of phase formation mechanisms at the interface between titanium and calcia-stabilized zirconia at 1550 °C, J. Am. Ceram. Soc. 93 (2010) 3893–3901.
[21] C.C. Lin, Y.W. Chang, K.L. Lin, K.F. Lin, Effect of yttria on interfacial reactions between titanium melt and hot-pressed yttria/zirconia composites at 1700 °C, J. Am. Ceram. Soc. 91 (2008) 2321–2327.
[22] K.L. Lin, C.C. Lin, Microstructural evolution and formation mechanism of the interface between titanium and zirconia annealed at 1550 °C, J. Am. Ceram. Soc. 89 (2006) 1400–1408.
[23] K.L. Lin, C.C. Lin, Reaction between titanium and zirconia powders during sintering at 1500 °C, J. Am. Ceram. Soc. 90 (2007) 2220–2225.

Cofinanciado por:
FCT Fundação para a Ciência e a Tecnologia
COMPETE 2020
PORTUGAL 2020
UNIÃO EUROPEIA
Fundo Europeu de Desenvolvimento Regional

[24] K.L. Lin, C.C. Lin, Effects of annealing temperature on microstructural development at the interface between zirconia and titanium, J. Am. Ceram. Soc. 90 (3) (2007) 893–899.
[25] L.D. Teng, F.M. Wang, W.C. Li, Thermodynamics and microstructure of Ti–ZrO_2 metal–ceramic functionally graded materials, Mater. Sci. Eng. A 293 (2000) 130–136.
[26] G. Miranda, et al., Design of Ti6Al4V-HA composites produced by hot pressing for biomedical applications, Mater. Des. 108 (2016) 488–493.
[27] Y. Yang, Q. Ma, Spark plasma sintering and hot pressing of titanium and titanium alloys, Titanium Powder Metallurgy: Science, Technology and Applications, 219, 2015.
[28] G. Bernard-Granger, et al., Spark plasma sintering of a commercially available granulated zirconia powder: comparison with hot-pressing, Acta Mater. 58 (9) (2010) 3390–3399.
[29] E. Zalnezhad, Effect of structural evolution on mechanical properties of ZrO_2 coated Ti–6Al–7Nb-biomedical application, Appl. Surf. Sci. 370 (2016) 32–39.
[30] J.-F. Lu, et al., Sintering Mechanism of Ti-6Al-4V Prepared by SPS, Appl. Mech. Mater. 782 (2015) 97.
[31] Z.A. Munir, D.V. Quach, M. Ohyanagi, Electric current activation of sintering: review of PECS, J. Am. Ceram. Soc. 94 (2011) 1–19.
[32] G. Jiang, D. Mishler, R. Davis, J.P. Mobley, J.H. Schulman, Zirconia to Ti-6Al-4V braze joint for implantable biomedical device, J. Biomed. Mater. Res. B Appl. Biomater. 72 (2) (2005) 316–321.
[33] I. Bespalov, M. Datler, S. Buhr, W. Drachsel, G. Rupprechter, Y. Suchorski, Initial stages of oxide formation on the Zr surface at low oxygen pressure: an in situ FIM and XPS study, Ultramicroscopy 159 (2015) 147–151.
[34] J. Wang, Y. Yu, S. Li, L. Guo, E. Wang, Y. Cao, Doping behavior of Zr4+ ions in Zr4+-doped TiO_2 nanoparticles, J. Phys. Chem. C 117 (2013) 27120–27126.
[35] A. Sinhamahapatra, J.P. Jeon, J. Kang, B. Han, J.S. Yu, Oxygen-deficient zirconia (ZrO_{2-x}): a new material for solar light absorption, Sci. Rep. 6 (2016) 27218, http://dx.doi.org/10.1038/srep27218.
[36] M. Esmaily, et al., Microstructural characterization and formation of α' martensite phase in Ti–6Al–4V alloy butt joints produced by friction stir and gas tungsten arc welding processes, Mater. Des. 47 (2013) 143–150.
[37] T. Ahmed, H.J. Rack, Phase transformations during cooling in α + β titanium alloys, Mater. Sci. Eng. A 243 (1) (1998) 206–211.
[38] P. Majumdar, S.B. Singh, M. Chakraborty, Elastic modulus of biomedical titanium alloys by nano-indentation and ultrasonic techniques—a comparative study, Mater. Sci. Eng. A 489 (1) (2008) 419–425.
[39] C. Santos, L.D. Maeda, C.A.A. Cairo, W. Acchar, Mechanical properties of hot-pressed ZrO_2–NbC ceramic composites, Int. J. Refract. Met. Hard Mater. 26 (2008) 14–18.
[40] P. Sevilla, C. Sandino, M. Arciniegas, J. Martínez-Gomis, M. Peraire, F.J. Gil, Evaluating mechanical properties and degradation of YTZP dental implants, Mater. Sci. Eng. C 30 (1) (2010) 14–19.